

Sample environment for in situ synchrotron corrosion studies of materials in extreme environments

Mohamed S. Elbakhshwan, Simerjeet K. Gill, Arthur T. Motta, Randy Weidner, Thomas Anderson, and Lynne E. Ecker

Citation: [Review of Scientific Instruments](#) **87**, 105122 (2016); doi: 10.1063/1.4964101

View online: <http://dx.doi.org/10.1063/1.4964101>

View Table of Contents: <http://scitation.aip.org/content/aip/journal/rsi/87/10?ver=pdfcov>

Published by the [AIP Publishing](#)

Articles you may be interested in

[Effect of current density on the microstructure and corrosion resistance of microarc oxidized ZK60 magnesium alloy](#)

Biointerphases **9**, 031009 (2014); 10.1116/1.4889734

[In situ fabrication of blue ceramic coatings on wrought Al Alloy 2024 by plasma electrolytic oxidation](#)

J. Vac. Sci. Technol. A **30**, 021302 (2012); 10.1116/1.3675610

[Comparative studies on the thermal stability and corrosion resistance of CrN, CrSiN, and Cr Si N/Al N coatings](#)

J. Vac. Sci. Technol. A **27**, 873 (2009); 10.1116/1.3155396

[Uniform Corrosion of Zirconium Alloy 4 Under Isothermal Oxidation at High Temperature](#)

AIP Conf. Proc. **989**, 73 (2008); 10.1063/1.2906098

[Surface characteristics and corrosion behavior of laser surface nitrided NiTi shape memory alloy for biomedical applications](#)

J. Laser Appl. **14**, 242 (2002); 10.2351/1.1514236



**COMPLETELY
REDESIGNED!**



**PHYSICS
TODAY**

Physics Today Buyer's Guide
Search with a purpose.

Sample environment for *in situ* synchrotron corrosion studies of materials in extreme environments

Mohamed S. Elbakhshwan,¹ Simerjeet K. Gill,^{1,a)} Arthur T. Motta,² Randy Weidner,¹ Thomas Anderson,¹ and Lynne E. Ecker¹

¹Nuclear Science and Technology Department, Brookhaven National Laboratory, Upton, New York 11973, USA

²Department of Mechanical and Nuclear Engineering, The Pennsylvania State University, University Park, Pennsylvania 16802, USA

(Received 29 June 2016; accepted 20 September 2016; published online 25 October 2016)

A new *in situ* sample environment has been designed and developed to study the interfacial interactions of nuclear cladding alloys with high temperature steam. The sample environment is particularly optimized for synchrotron X-ray diffraction studies for *in situ* structural analysis. The sample environment is highly corrosion resistant and can be readily adapted for steam environments. The *in situ* sample environment design complies with G2 ASTM standards for studying corrosion in zirconium and its alloys and offers remote temperature and pressure monitoring during the *in situ* data collection. The use of the *in situ* sample environment is exemplified by monitoring the oxidation of metallic zirconium during exposure to steam at 350 °C. The *in situ* sample environment provides a powerful tool for fundamental understanding of corrosion mechanisms by elucidating the substoichiometric oxide phases formed during the early stages of corrosion, which can provide a better understanding of the oxidation process. Published by AIP Publishing. [<http://dx.doi.org/10.1063/1.4964101>]

INTRODUCTION

Corrosion of zirconium alloy fuel cladding in water or steam and the associated hydrogen pickup is a limiting factor for increasing fuel burn-up in current and future reactors.^{1–12} The hydrogen pickup associated with the corrosion process can embrittle the cladding by hydride formation. The corrosion of zirconium alloys occurs at the metal/oxide interface.^{1–3} The current model of zirconium alloy corrosion is that a protective layer of zirconium oxide forms at the interface. The protective nature of the oxide layer decreases at the oxide transition, thought to be caused by an accumulation of stress in the growing oxide. This phenomenon is cyclic and occurs several times during the life of a fuel rod. Zirconium alloys with slightly different compositions and microstructures show widely different corrosion behaviors. Such differences are manifested in the corrosion rate and on the thickness at which the oxide transition occurs and are likely caused by differences in oxide microstructure.^{1–3}

There is a lack of fundamental understanding of oxidation and associated corrosion mechanisms that occur at zirconium alloy cladding interfaces under extreme conditions of temperature, pressure, and corrosive environments.^{1,2} For most metal-oxide systems, the relationships between the oxidation conditions and the resulting oxide-film growth kinetics and microstructure are poorly understood.³ Several studies using surface sensitive methods (STM, TEM, and XPS) have been done.^{13–19} However, there is limited information about the structural changes as well as the change in the elemental distribution at the early oxidation stages of oxide-film growth. This knowledge gap can be addressed by

developing advanced sample environments where material interactions and behavior at the surfaces and interfaces can be studied *in situ* under corrosive conditions. Such understanding is vital to predict the performance of existing claddings and to design and develop materials with long-lived stability under extreme conditions.²⁰ High synchrotron X-ray energy and brightness, coupled with advanced sample environments, present an exceptional opportunity to understand the fundamental interfacial processes involved in the degradation of materials in extreme environments.^{3,6,11,12}

In our work, we demonstrate the capabilities of an *in situ* sample environment that we developed to monitor oxidation at zirconium alloy-steam interfaces under corrosive conditions using *in situ* synchrotron X-ray diffraction (XRD). The *in situ* sample environment provides the capability of precisely controlling the temperature during oxidation using a LabVIEW-based platform. The environment has the ability to monitor corrosion both in transmission and reflection geometry for bulk and surface structural analysis. In addition, the dimensions of the microreactor where the sample is mounted comply with G2 ASTM standard²¹ for studying corrosion in zirconium and zirconium-based alloys making the results collected relevant to industrial conditions and directly comparable to autoclave testing. In this article, we present the *in situ* corrosion data collected on metallic zirconium in steam at 350 °C and elucidate the structure of oxide phases formed at the very beginning of corrosion.

Clearly, applications of the *in situ* sample environment are not limited to corrosion of nuclear claddings. It includes studying corrosion in materials relevant to many energy sector areas such as hydrogen storage, batteries, CO₂ sequestration, and geothermal wells. It also includes studying interfacial interactions on surface modified materials such as corrosion resistant coatings and advanced structural ceramics. All these

^{a)}Author to whom correspondence should be addressed. Electronic mail: gills@bnl.gov. Tel.: 631-344-5633. Fax: 631-344-7650.

materials are of high technological value often are complex, nanostructured, and heterogeneous and involve exposure to extreme environments.^{22–24} Neither is the application of *in situ* sample environment limited to the XRD analysis.

THE DESIGN OF THE *IN SITU* SAMPLE ENVIRONMENT

The *in situ* sample environment developed will provide nanoscale monitoring for material-fluid interfaces in real time using advanced X-ray nano and micro beams at synchrotron facilities. The scope of the sample environment is broad and can be extended to all the energy sectors that involve the understanding of metal alloy-fluid interface including steam and supercritical carbon dioxide environments. The sample environment design is sufficiently flexible to adapt to various beamline set ups, where the surface orientation required for *in situ* data collection might be horizontal or vertical relative to the beam direction.

The sample environment design consists of three main parts: (1) the reaction cell, (2) the delivery system, and (3) the instrumentation and control loop as shown in Figure 1. The reaction cell is where the sample is mounted and actual corrosion takes place when the steam is delivered into it by the delivery system. The delivery system consists of a pressurizer, a tubing, and a distribution system for steam generation and delivery. The instrumentation and control loop is a LabVIEW-based platform for remote monitoring of temperature and pressure of the reaction cell and the delivery system while the *in situ* sample environment is in operation.

The reaction cell

The overall design of the reaction cell is based on a modified Merrill-Bassett type diamond anvil cell to assemble all parts in a compact form,^{22,25} as shown in Figure 2. It consists of four major parts: Outer frame, microreactor, sample holder, and sealing windows. The design of the reaction cell was modified from an existing *in situ* environment developed by Diefenbacher *et al.*²² for *in situ* spectroscopic and diffraction studies of mineral carbonation and CO₂ sequestration under supercritical carbon dioxide environments.^{23,24} The reaction cell was modified to investigate the corrosion of zirconium-based claddings where cell dimensions complied with G2 ASTM industrial standard for corrosion tests of zirconium alloys.²¹ The total volume of reaction cell was designed to be 100 μl and sample surface area to cell volume ratio was designed to be 0.1 m^2/l .

The outer frame is made up of Vascomax (300 steel alloy) which has high strength but lower corrosion resistance than Hastelloy. It is easier to machine and has lower density which reduces the overall cost and weight of the reaction cell. It holds the windows, gaskets, and micro-reactor core together by screws that hold them between the two parts of the triangular frame.

The micro-reactor core has a cylindrical diameter of 5 mm and 10 mm length, with grooves to support the sample holders in the center to assure uniform oxidation on both sides of the sample. It has an opening angle of 38° to allow for both transmission and reflection XRD measurements as shown in Figure 3. At both ends of the cylindrical core, 10 mm diameter and 2 mm deep holes were created to accommodate

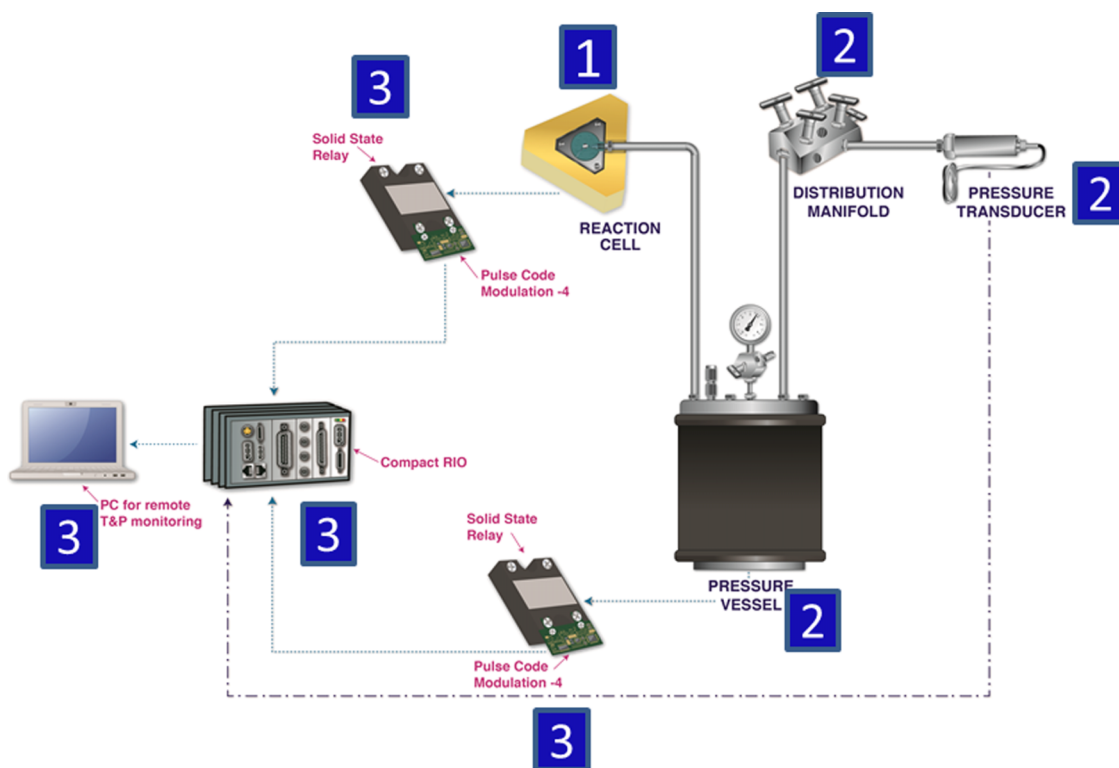


FIG. 1. Schematic showing three major components of the *in situ* sample environment (1) the reaction cell, (2) delivery system along with (3) LabVIEW-based instrumentation and control loop.

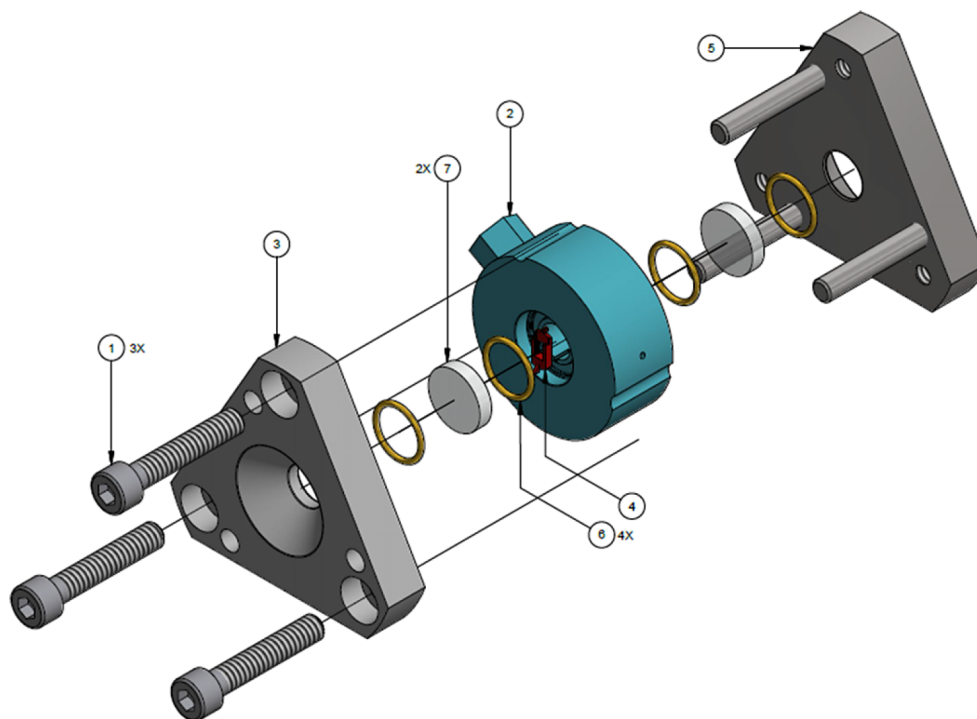


FIG. 2. The components of the core of the sample environment. The components are: (1) bolts, (2) the reaction cell, (3) the outer frame (upper plate), (4) the sample holder, (5) the outer frame (lower plate), (6) O-ring or gasket, and (7) windows.

the sealing windows. It holds the sample holder where the sample is mounted. Both the microreactor core and sample holders are made from Hastelloy C22 in order for them to be corrosion resistant in steam, an environment that nuclear

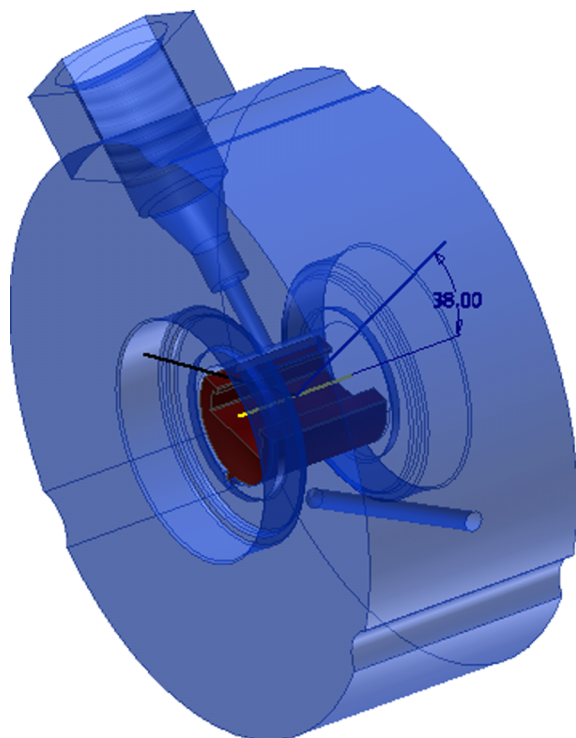


FIG. 3. The opening angle of the core. This determines the angle of X-rays coming from the sample that can be collected at the detector. It was optimized to provide enough structural support and to accommodate spectroscopy measurements in the fluorescence mode.

claddings are exposed to in a typical boiling water nuclear reactor. The microreactor has an inlet where the steam is delivered from the pressurizer through 1/16 in. stainless steel high performance liquid chromatography (HPLC) tubing which is connected to the core through internal 10–32 threads connection. In addition, it is equipped with thermocouple which is placed inside the microreactor frame and monitors the temperature on the micro-reactor. The sample temperature is measured using this grounded thermocouple embedded into the core body without penetrating the interior to provide accurate reading of the sample temperature. It is placed in 0.42 mm diameter opening that extends from the outer surface core up to the edge of the sample chamber as shown in Figure 3.

The sample holder has two different designs for *in situ* data collection: transmission mode holder (as shown in Figure 4(a)) which holds the sample perpendicular to the X-ray beam and reflection mode holder (as shown in Figure 4(b)) which holds the sample parallel to the X-ray beam. The transmission geometry allows structural measurement of both the bulk sample and thick oxide films that are formed during corrosion. However, if the oxide film is very thin compared to the bulk sample, the diffraction pattern is dominated by the bulk signal with very little or even unmeasurable contribution from the newly developed oxide layer. The reflection mode holder allows the sample surface to be parallel to the beam which is suitable to perform grazing incidence diffraction measurements as shown in Figure 4(b). This technique is most effective in detecting the development of newly formed thin oxide films on the surface of the sample.

For the sealing windows, Single crystal moissanite and sapphire windows were selected for high energy XRD measurements while glassy carbon windows were selected

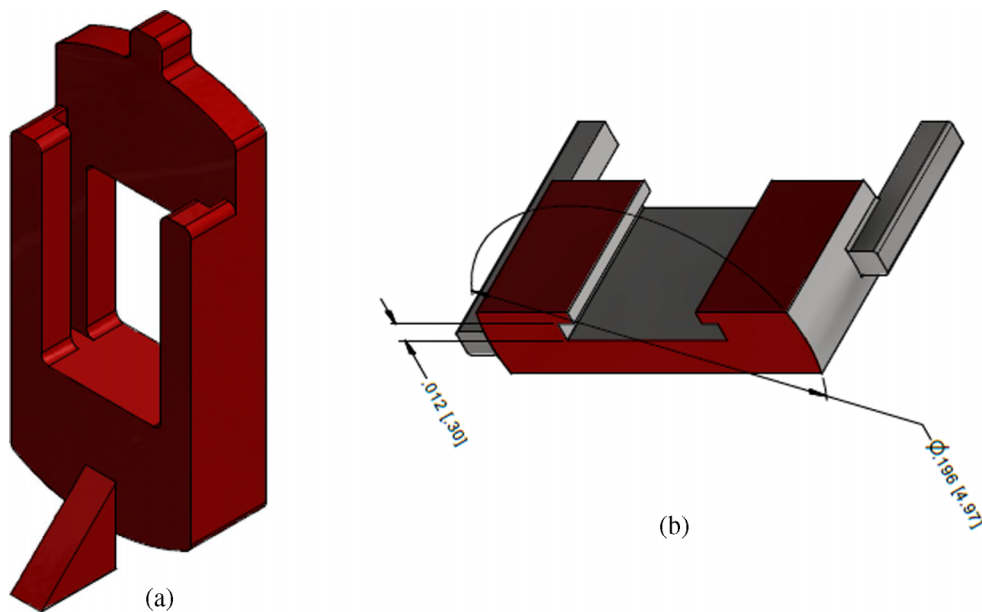


FIG. 4. (a) Transmission and (b) reflection sample holder.

for low energy measurements.²⁶ Flexural strength calculations were performed to ensure that windows met the requirements to withstand the high pressure operating conditions during *in situ* data collection. The optimum thickness of the windows was found to be 2 mm to provide enough strength to withstand the high pressure and in the same time to the transmission of reliable X-ray signal during measurements. For initial testing for windows, a sample was sandwiched by two windows at each side to simulate the sample environment conditions. Single crystal moissanite showed two minor peaks, while glassy carbon gave five broad peaks with high background especially in the low 2θ range as shown in Figure 5.

The reaction cell is sealed by placing flat circular gaskets with outer diameters of 8.89 mm and thickness of 0.6 mm between the cell core and the windows. Additional gaskets are placed between the windows and the frame to reduce friction between windows and outer frame and protect the windows

as shown in Figure 2. Both gold and annealed aluminum gaskets were used due to the softness and durability at high temperatures (up to 400 °C) and being chemically inert with steam environments. Pre-rated torque is used to seal the reaction cell applied equally to three bolts located at each corner of the triangular cell.

Once the reaction cell is assembled the heating of the cell is performed using a copper-based heater where the temperature on the reaction cell is controlled independently from the pressure vessel. A hollow triangular copper-based heater was built to surround the reaction cell from all directions except the faces with the windows to allow the passage of the X-rays as shown in Figure 6. Total of five cartridge heaters with different power ratings were embedded in the copper heating block through the three sides to assure uniform heating of the reaction cell. A large opening was cut at one side to allow a position for the steam inlet and

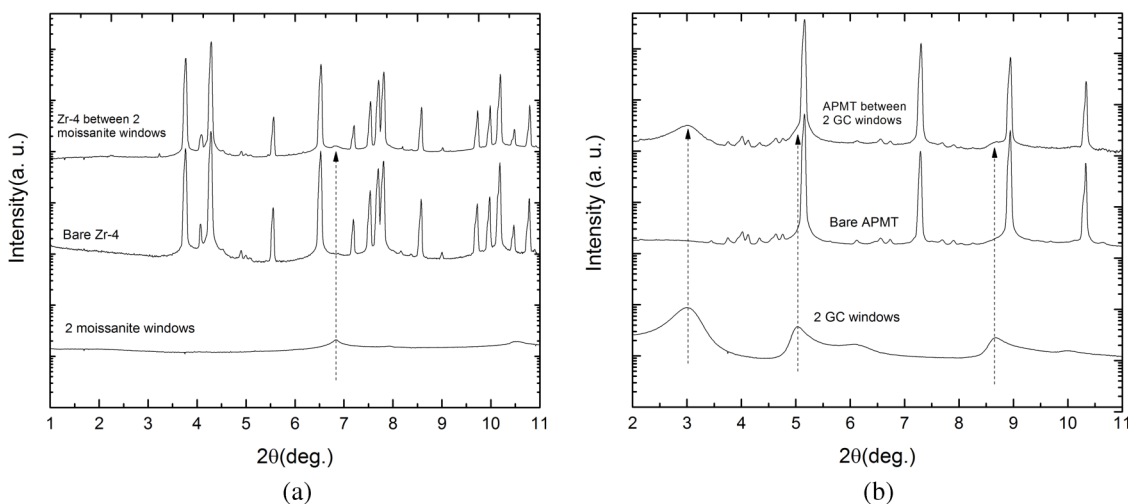


FIG. 5. XRD patterns for (a) moissanite windows with zirconium alloy and (b) glassy carbon windows with advanced steel. Data were collected at X-ray wavelength of 0.1839 Å.

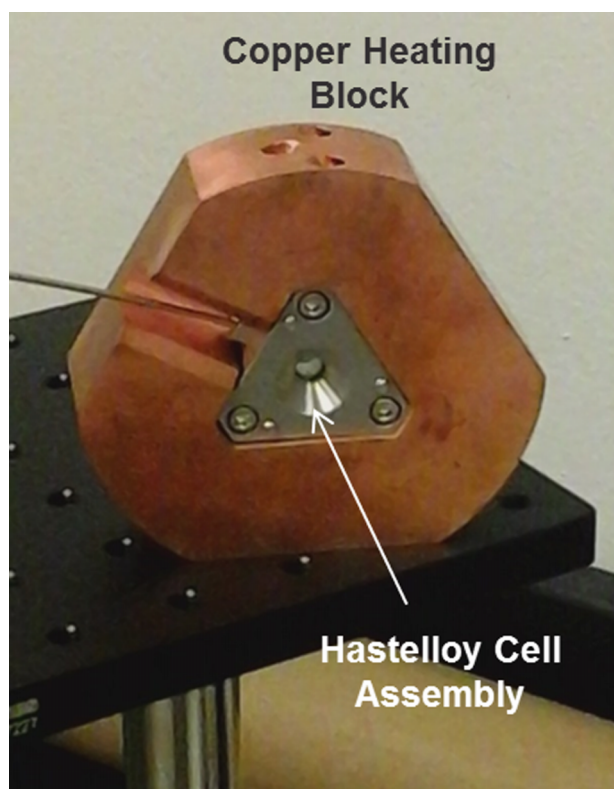


FIG. 6. Image showing the copper heating block surrounding the Hastelloy reaction cell.

another opening was placed to allow a channel to place the thermocouple of the reaction cell.

The delivery system

The delivery system is used for both steam generation and delivery during *in situ* corrosion experiments. It consists of three major components: a pressure vessel, a distribution manifold, and a pressure transducer. The pressure vessel is where the steam is generated for corrosion studies, distribution manifold is used to flow the steam in the *in situ* sample environment, and pressure transducer is used for communicating with instrumentation and control loop for the remote monitoring of pressure and temperature.

The *pressure vessel* plays the role of the steam generator as well as the pressure controller of the whole system. The water flows through 1/4 in. stainless steel tubing to the pressure vessel which acts as the steam generator in the system. For steam generation, the *in situ* sample environment is evacuated followed by introducing deionized water into the pressurizer which is heated using the heater jacket surrounding the pressurizer. The steam generated then fills the *in situ* sample environment including the delivery system and reaction cell, making the pressurizer as the main point of pressure control. The pressure vessel is ASTM rated up to 2950 psi at 350 °C and it is equipped with two built-in Alloy C-276 rupture discs as a safety barrier against over pressurizing.

The *distribution manifold* is used for controlling the fluid flow in the system. It has 5 valves and each valve is used for specific function during the operation of *in situ* sample environment which includes evacuating the

system, introducing water in pressurizer for steam generation, introducing other components in case mixture was to be used as a corrosive environment, and communicating with instrumentation loop via pressure transducer.

The *pressure transducer* generates an electrical signal to the LabView-based instrumentation loop (see below) as a function of the pressure imposed, which enables remote monitoring of pressure outside the hutch during the *in situ* corrosion data collection. The pressure transducer chosen is rated up to 300 °C, while the temperature measured near transducer connection was 315 °C when *in situ* sample environment is in operation. Hence, a cooling tower was introduced to compensate for the temperature difference as shown in Figure 7.

The instrumentation and control loop

The instrumentation and control loop allows remote monitoring of temperature and pressure outside the hutch during the *in situ* data collection. It has two main components Compact Rio (CRio) and PCM4s. The *CRio* is the main hardware platform for running the LabView real time software as shown in Figure 1. The software is used to control the hardware, display, and store parameter (T, P) information, while the *in situ* data collection it monitors temperature readouts of the pressure vessel and the reaction cell from the thermocouples in the copper-based heater on the reaction cell and the pressure vessel and outputs two individual 4–20 mA DC signals, respectively, to Omega Pulse Control Module (PCM4s).

The *PCM4s* convert the 4–20 mA signals to voltage which is read by the solid state relays (SSRs). The SSRs control the heaters on both the reaction cell and pressure vessel using this time proportional voltage output. Linearly from 20 mA to 4 mA the SSR goes from fully closed (20 mA) to completely open (4 mA). The instrumentation and control system is also setup to be able to manually control the 4–20 mA signal so the user can control the rate of the temperature increase manually.

During the development of *in situ* sample environment, safety by design approach was followed and many in-built safety features were introduced. The first feature is that the pressure and temperature are compared against one another using a modified ASME steam table. If the temperature's related ASME steam table pressure and the actual system pressure are off by ± 50 psi (gauge) an alarm is triggered. This enables safe operation if there is a sudden drop in pressure due to leak during *in situ* corrosion data collection. Second, the *in situ* sample environment has a manual safety built into the software that allows the user to power off the heaters for the reaction cell and the pressure vessel if required. Third, the system is setup to automatically turn off power to the heaters in case of a large decrease in the pressure occurs. This function was designed to prevent complete drying of pressurizer and keeping system safe in case of disc rupture.

IN SITU CORROSION STUDY

As a preliminary step, initial testing of the *in situ* sample environment was done at the X17A beamline in the National

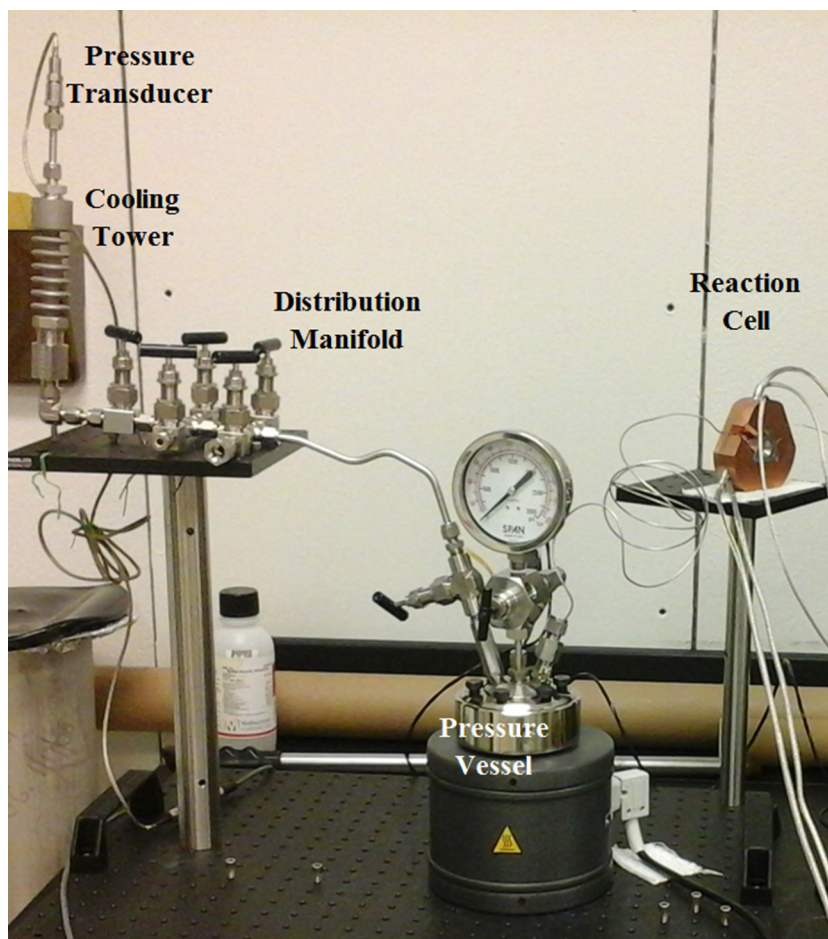


FIG. 7. Image showing the actual reaction cell, pressure vessel, pressure transducer, cooling tower, and the distribution manifold.

Synchrotron Light Source (NSLS). An *in situ* corrosion study of metallic zirconium under steam at 250 °C and 600 psi was carried out successfully for 31 h. The X-ray wavelength was 0.1839 Å and beam size was 500 × 500 μm². We were able to collect *in situ* data with good sealing using moissanite windows. No oxide peaks were noticed due to the short exposure time and low temperature; however, a successful leak free test and *in situ* corrosion data collection in transmission geometry were achieved.

After successful demonstration of sample environment for *in situ* corrosion data collection under steam environment, an *in situ* corrosion study of zirconium metal under steam was carried out using Zr metal at 6-ID-D beamline at the Advanced Photon Source (APS) in Argonne National Laboratory. The data were reduced using Nika software.²⁷ The specimen was exposed to steam at 350 °C and 50 psi for 82 h. The specimen had a surface area of 2 × 2 mm² with 200 μm thickness. The measurements were collected using grazing incidence geometry using the reflection sample holder shown in Figure 4(b). The X-ray wavelength was 0.1235 Å and beam was reduced in the vertical direction to 70 μm while the beam width was 200 μm. The specimen was aligned parallel to the beam while touching only the lower portion of it. The surface sensitivity of the measurements was optimized on the sample by changing the tilt angle of the sample (0.3°–2°) while monitoring the intensity of the oxide peak. This procedure

was used to maximize the signal from the slowly grown oxide layer relative to the bulk. For each pattern, the specimen was exposed to the X-ray beam for 10 s and a total of 20 exposures were summed together to give one pattern. Two references were used to calibrate the sample to detector distance: first, Ni NIST standard powder wrapped in a Kapton tape and placed inside the sample environment. This calibration was used as a guide for the sample position with respect to the detector. Once the *in situ* data collection was started the Zr metal peaks were used to calibrate the sample to detector distance to avoid any effect of the sample movement (if any) on the data analysis. In these measurements, single crystal sapphire windows were used to seal the sample environment. The windows contributed two sharp peaks to the diffraction pattern, while the sample holder (made from Ni-based alloy “Hastelloy C22”) added a total of six peaks to the patterns as shown in Figure 8. Such interference could be eliminated if a smaller X-ray beam can be used.

After exposure to steam for 32 h, the development of four non-stoichiometric oxide peaks was observed at the diffraction angles of 0.92°, 1.54°, 1.75°, and 2.3° which can be attributed to the growth of the Zr₃O, Zr₃O_{1-x}, and Zr₃O_{1-x} oxide phases as shown in Figure 9. Our findings of formation and growth of non-stoichiometric oxide film with an overall O/Zr-ratio < 2 are consistent with previous studies.^{17–19} The initial formation of thin oxide film on zirconium metal surface involves various

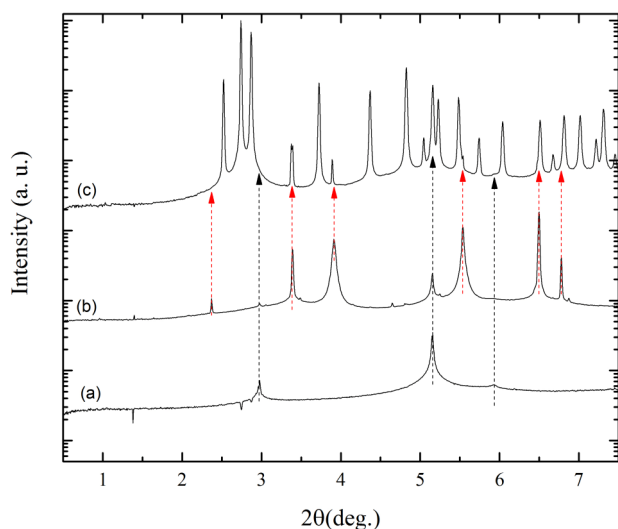


FIG. 8. XRD pattern for (a) sapphire windows, (b) sapphire windows with the sample holder, and (c) sapphire windows, the sample holder, and Zr metal specimen. Black arrows point to diffraction peaks from the windows while red arrows point to diffraction peaks from the sample holder. Data were collected at X-ray wavelength of 0.1235 Å.

steps which include transport of oxygen molecules to the surface followed by their adsorption, which is followed by oxide nucleation and growth, subsequently resulting in the formation of a protective oxide film covering the entire metal surface, and continued oxide-film growth.^{1,2} The formation of non-stoichiometric phase at the initial stage comes from a concentration gradient of Zr-enrichment and O-deficiency in the developing oxide film that decreases from metal/oxide interface towards the oxide surface.^{17,18} These results show that at the early stages of oxidation, there is not enough oxygen at the interface to form the stable monoclinic zirconium oxide. This is due to the slow diffusion kinetics (due to low temperature and short amount of time) for oxygen ions that are being transferred through the zirconium surface.^{17–19,28} Beyond the first 40 h of exposure, the diffraction patterns showed the development of the tetragonal and monoclinic

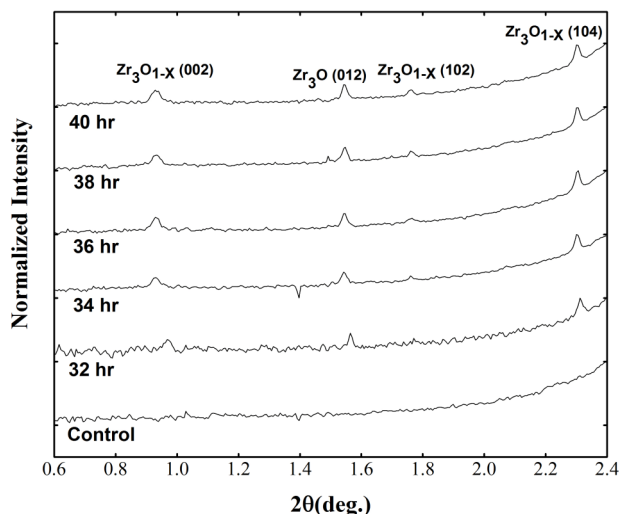


FIG. 9. XRD patterns of Zr metal exposed to steam at 350 °C and 50 psi up to 40 h. Data were collected at X-ray wavelength of 0.1235 Å.

zirconium oxide peaks when the suboxide peaks disappeared, and these data will be discussed in more detail in future publications.

CONCLUSION

A novel *in situ* sample environment for monitoring structural changes and oxide growth on nuclear cladding steam interfaces using high resolution synchrotron methods was designed and built. The first results of *in situ* data collection are presented here as an initial step toward developing a technique capable of *in situ* studies of variety of zirconium-based and other advanced cladding alloys in corrosive environments of steam and supercritical carbon dioxide. We were able to successfully monitor the substoichiometric oxide phases formed during the initial corrosion of zirconium in steam at 350 °C. The environmental cell design offers great flexibility and can be used to study a variety of material interfaces under extreme environments at the nanoscale. The design allows for studies of numerous interfacial phenomena including oxidation of thin films, hydride formation, and detection of early oxidation forms. Such information can be gained not only in pure steam environments but also with different additives and under various environments including supercritical carbon dioxide. The ability to couple high resolution synchrotron methods for *in situ* analysis using this new *in situ* sample environment opens up a large number of possibilities for mechanistic corrosion studies under extreme environments.

ACKNOWLEDGMENTS

The authors would like to thank Andrew Desantis for CAD drawing, Hengzi Wang for designing the grazing incidence sample holder. The authors would like to thank Dr. Sanjit Ghose, Dr. Eric Dooryhee from XPD/NSLS-II beamline and Dr. Juergen Thieme from SRX/NSLS-II for optimizing the cell design for the beamline measurements, and Michael Gaffney's team at NSLS-II for discussion about safety features in the cell design. Special thanks to Dr. Douglas Robinson; the beamline scientist at 6-ID-D beamline in the Advanced Photon Source, for his patience and dedication during the data collection. This work was supported by Laboratory Directed Research and Development (LDRD) Program (Project No. 13-027) at BNL. Work at the NSLS and CFN was supported under US DOE Contract No. DE-AC02-CH10886. This research used resources of the Advanced Photon Source, a U.S. Department of Energy (DOE) Office of Science User Facility operated for the DOE Office of Science by Argonne National Laboratory under Contract No. DE-AC02-06CH11357. CHESS is supported by the NSF & NIH/NIGMS via NSF Award No. DMR-1332208.

¹A. Motta, A. Couet, and R. Comstock, "Corrosion of zirconium alloys used for nuclear fuel cladding," *Annu. Rev. Mater. Res.* **45**(1), 311–343 (2015).

²A. Motta, "Waterside corrosion in zirconium alloys," *JOM* **63**(8), 59–63 (2011).

³A. Yilmazbayhan, M. Gomes, A. Motta, H. Kim, Y. Jeong, J. Park, R. Comstock, B. Lai, and Z. Cai, "Characterisation of oxides formed on model zirconium alloys in 360 °C water using micro-beam

- synchrotron radiation,” in *Proceedings of 12th International Conference on Environmental Degradation of Materials in Nuclear Power Systems—Water Reactors* (TMS, 2005), p. 201.
- ⁴A. Couet, A. Motta, and A. Ambard, “The coupled current charge compensation model for zirconium alloy fuel cladding oxidation: I. Parabolic oxidation of zirconium alloys,” *Corros. Sci.* **100**, 73–84 (2015).
- ⁵X. Iltis, F. Lefebvre, and C. Lemaignan, “Microstructural study of oxide layers formed on zircaloy-4 in autoclave and in reactor part I: Impact of irradiation on the microstructure of the zirconia layer,” *J. Nucl. Mater.* **224**, 109–120 (1995).
- ⁶D. Spengler, A. Motta, R. Bajaj, J. Seidensticker, and Z. Cai, “Characterization of zircaloy-4 corrosion films using microbeam synchrotron radiation,” *J. Nucl. Mater.* **464**, 107–118 (2015).
- ⁷A. Couet, A. Motta, and R. Comstock, “Hydrogen pickup measurements in zirconium alloys: Relation to oxidation kinetics,” *J. Nucl. Mater.* **451**(1-3), 1–13 (2014).
- ⁸A. Parkison and A. Nelson, “Hydrogen measurement during steam oxidation using coupled thermogravimetric analysis and quadrupole mass spectrometry,” *Measurement* **82**, 391–402 (2016).
- ⁹B. Cox, “Some thoughts on the mechanisms of in-reactor corrosion of zirconium alloys,” *J. Nucl. Mater.* **336**, 331–368 (2005).
- ¹⁰V. Urbanic and T. Heidrick, “High-temperature oxidation of zircaloy-2 and zircaloy-4 in steam,” *J. Nucl. Mater.* **75**, 251–261 (1978).
- ¹¹E. Polatidis, P. Frankel, J. Wei, M. Klaus, R. Comstock, A. Ambard, S. Lyon, R. Cottis, and M. Preuss, “Residual stresses and tetragonal phase fraction characterisation of corrosion tested zircaloy-4 using energy dispersive synchrotron X-ray diffraction,” *J. Nucl. Mater.* **432**, 102–112 (2013).
- ¹²W. Mohamed, D. Yun, K. Mo, M. Pellin, M. Billone, J. Almer, and A. Yacout, “Depth profile of oxide volume fractions of zircaloy-2 in high-temperature steam: An *in-situ* synchrotron radiation study,” *J. Nucl. Mater.* **454**(1-3), 192–199 (2014).
- ¹³G. Bakradze, L. Jeurgens, and E. Mittemeijer, “An STM study of the initial oxidation of single-crystalline zirconium surfaces,” *Surf. Sci.* **606**, 846–851 (2012).
- ¹⁴G. Bakradze, L. Jeurgens, and E. Mittemeijer, “The different initial oxidation kinetics of Zr(0001) and Zr(1010) surfaces,” *J. Appl. Phys.* **110**, 024904 (2011).
- ¹⁵Y. Nishino, A. Krauss, Y. Lin, and D. Gruen, “Initial oxidation of zirconium and zircaloy-2 with oxygen and water vapor at room temperature,” *J. Nucl. Mater.* **228**, 346–353 (1996).
- ¹⁶B. Zhou, J. Peng, M. Yao, Q. Li, S. Xia, C. Du, G. Xu, P. Barberis, and S. Dean, “Study of the initial stage and anisotropic growth of oxide layers formed on zircaloy-4,” *J. ASTM Int.* **8**(1), 102951 (2011).
- ¹⁷A. Lyapin, L. Jeurgens, and E. Mittemeijer, “Effect of temperature on the initial, thermal oxidation of zirconium,” *Acta Mater.* **53**(10), 2925–2935 (2005).
- ¹⁸L. Jeurgens, A. Lyapin, and E. Mittemeijer, “The initial oxidation of zirconium—Oxide-film microstructure and growth mechanism,” *Surf. Interface Anal.* **38**, 727–730 (2006).
- ¹⁹A. Lyapin, L. Jeurgens, P. Graat, and E. Mittemeijer, “The initial, thermal oxidation of zirconium at room temperature,” *J. Appl. Phys.* **96**(12), 7126–7135 (2004).
- ²⁰Basic Research Needs for Materials under Extreme Environments, Report for DOE Office of Basic Energy Sciences, 2007.
- ²¹ASTM standards, G2/G2M–06, Corrosion Testing of Products of Zirconium, Hafnium, and Their Alloys in Water at 680 °F or in Steam at 750 °F, 2011.
- ²²J. Diefenbacher, M. McKelvy, A. Chizmeshya, and G. Wolf, “Externally controlled pressure and temperature microreactor for *in situ* x-ray diffraction, visual and spectroscopic reaction investigations under supercritical and subcritical conditions,” *Rev. Sci. Instrum.* **76**(1), 015103 (2005).
- ²³T. Kim, T. Tokunaga, D. Shuman, S. Sutton, M. Newville, and A. Lanzirotti, “Thickness measurements of nanoscale brine films on silica surfaces under geologic CO₂ sequestration conditions using synchrotron X-ray fluorescence,” *Water Resour. Res.* **48**(9), 1–13, doi:10.1029/2012WR012200 (2012).
- ²⁴T. Kim, T. Tokunaga, J. Bargar, M. Latimer, and S. Webb, “Brine film thicknesses on mica surfaces under geologic CO₂ sequestration conditions and controlled capillary pressures,” *Water Resour. Res.* **49**(8), 5071–5076, doi:10.1002/wrcr.20404 (2013).
- ²⁵L. Merrill and W. Bassett, “Miniature diamond anvil pressure cell for single crystal x-ray diffraction studies,” *Rev. Sci. Instrum.* **45**(2), 290–294 (1974).
- ²⁶S. Griesel, U. Reus, and A. Prange, “Electro-deposition as a sample preparation technique for total-reflection X-ray fluorescence analysis,” *Spectrochim. Acta, Part B* **56**, 2107–2115 (2001).
- ²⁷J. Ilavsky, “Nika: Software for two-dimensional data reduction,” *J. Appl. Crystallogr.* **45**, 324–328 (2012).
- ²⁸L. Jeurgens, A. Lyapin, and E. Mittemeijer, “The mechanism of low-temperature oxidation of zirconium,” *Acta Mater.* **53**(18), 4871–4879 (2005).